Prediction of Vibrational Frequencies of Possible Intermediates and Side Products of the Methanol Synthesis on ZnO($000\overline{1}$) by Ab Initio Calculations

Jörg Koßmann,[a] Guido Roßmüller, and Christof Hättig

Lehrstuhl für Theoretische Chemie, Ruhr-Universität Bochum, D-44780 Bochum, Germany

(Dated: November 21, 2011)

We used *ab initio* density functional theory in combination with an embedded cluster approach to calculate vibrational spectra and formation enthalpies of possible intermediates and side products (spectator species) in the synthesis of methanol out of syn gas on the ZnO($000\overline{1}$) surface. Our investigations base upon our previous work on possible reaction pathways and activation barriers for this reaction at oxygen vacancies on ZnO($000\overline{1}$). We present and discuss calculated vibrational frequencies of short-living formyl, hydroxymethylene, formaldehyde, acetale and hydroxymethyl intermediates and compare the calculated frequencies of formate and methoxy species as well as CO and CO_2 species, at the defect free surface and at oxygen vacancies, with recent experimental findings. All investigated species show characteristic features in their spectra. Therefore the analysis of their vibrational frequencies is a suitable mean to distinguish them and gain new insights in this reaction which is of recent experimental interest. We are able to identify the structure and characteristics of different surface species, like monodentate and polydentate carbonate and formate species, in agreement with experimental results.

Keywords: catalysis, density functional theory, embedded cluster method, adsorbates, zinc oxide, spectroscopy

[a]To whom correspondence should be addressed. email: joerg.kossmann@theochem.ruhr-uni-bochum.de

I. INTRODUCTION

In the industrial synthesis of methanol out of syngas a mixture of copper, zinc oxide, and Al_2O_3 is used as catalyst[1]. In this system ZnO is used as support material, but it has been shown that zinc oxide can itself act as active component in this heterogeneous catalysis process[2]. When pure zinc oxide is used as catalyst, the ZnO$(000\overline{1})$ surface exhibits the highest activity in the methanol synthesis[3,4]. Hence different reaction path ways have been suggested assuming oxygen vacancies on ZnO$(000\overline{1})$ as the active center and details of the possible mechanisms have been discussed controversially in recent literature[5–9].

Although syngas, generated by steam reforming, consists mainly of CO and H_2, already due to the Boduard equilibrium and the water gas shift reaction, there is always a small amount of carbon dioxide in the gasphase of the real catalytic system. Furthermore, syngas obtained from biomass, which can also be used for methanol synthesis[10], might differ in its composition and have a higher CO_2 content. And in fact, CO_2 is the carbon source in the methanol synthesis on many metal oxide catalysts[11] and also on a copper single crystal surface[12]. This is especially also the case for $Cu/Al_2O_3/ZnO$ catalyst mixtures[13]. Hence one can easily come up with the idea of assuming that also at copper free ZnO$(000\overline{1})$ surfaces CO_2 might be the carbon source in this reaction, and indeed some reaction models follow this assumption[14]. But recent investigations have proven that CO_2 – even in low concentrations – act in fact inhibitor for the methanol synthesis at copper free ZnO catalysts[8], making it more likely that in these systems carbon monoxide is the only carbon source. The same studies show that in the presence of copper CO_2 is no longer an inhibitor for the reaction. In the present work we investigated CO as well as CO_2 adsorbates at the defect free surface and at oxygen vacancies on ZnO$(000\overline{1})$.

Formate species have been discussed as intermediates or side products of the methanol synthesis on ZnO$(000\overline{1})$ surfaces[8,9]. This idea is supported by experiments, in which formate species could be observed during the methanol oxidation[15] and after methanol adsorption at $Cu/ZnO/Al_2O_3$ catalysts[16,17] and at clean ZnO and Au/ZnO nanoparticles[18]. In the methanol synthesis process, formate species can be formed through the reduction of CO_2 by dissociatively adsorbed H_2 or by the formal insertion of CO in a surface OH group.

Similar to formate species, also formyl species are possible intermediates of the methanol

synthesis. They are accessible through the reduction of adsorbed CO molecules by a simultaneous transfer of a proton and an electron pair to the adsorbate. It has been shown that a formyl species at an F^{2+} center is less favourable than formyl species at F centers[7] where the carbon atom is bound to a surface zinc atom. So far, formyl species could not be observed experimentally as intermediates in the methanol synthesis, but this might be a consequence of the short life time of these species, which is supported by the predicted low reaction barriers to subsequent intermediates[7]. To assist the experimental identification of such formyl species we computed at $F^{2+}$and F vacancies their structures, enthalpies of formation, and vibrational frequencies.

As already mentioned, formaldehyde can be formed as a possible further intermediate or a side product in the methanol synthesis. It can be physisorbed at the surface as a rather weakly bound formaldehyde species, which might react further into a hydroxymethyl species by abstracting a hydrogen atom from a surface OH group. Alternatively the oxygen atom of formaldehyde can react with an electron deficient F^{2+} vacancy into acetale species.

Obviously, a final step in the methanol synthesis should be forming a kind of methanol species, probably by the protonation of a surface methoxy intermediate. Such surface methoxy species occur after methanol adsorption on $Cu/ZnO/Al_2O_3$ catalysts[15,16] and on ZnO single crystal surfaces, including $ZnO(000\overline{1})$[19]. Also at clean ZnO and Au/ZnO nanoparticles the formation of methoxy species after exposition to methanol could be confirmed in a recent study[18].

In our previous study reported in Ref. 7 we have extensively studied the possible reaction pathways of the methanol synthesis at an oxygen vacancy on $ZnO(000\overline{1})$ together with the transition states and activation barriers. In order to get further insight into the reaction mechanism, a combination of theoretical and experimental work is certainly necessary in order to interpret spectroscopic results from infra red (IR) measurements and high resolution electron energy loss spectroscopy (HR-EELS) at single crystal surfaces and IR studies at powders. Especially in the latter case, *in situ* infra red measurements, like those reported in Ref. 15, could be extremely helpfull. But to characterize intermediates, a comparison to calculated vibrational spectra is needed.

The goal of the present work is to complement the work of Ref. 7 by a detailed theoretical

study of the vibrational spectra of species which might be observed in the course of such in situ IR measurements. Therefore we study in addition to intermediates and the main reaction path way also side products, spectator species, and stable intermediates of unfavored reaction path ways, as e.g. formyl, formate, hydroxymethylene, formaldehyde, acetale, hydroxymethyl and methoxy species at the ZnO($000\overline{1}$) surface. The main focus was thereby on the prediction of the vibrational spectra, which serve as reference for future assignments of vibrational frequencies measured in experimental studies.

II. COMPUTATIONAL DETAILS

In order to obtain vibrational frequencies and binding enthalpies of adsorbates we performed embedded cluster calculations in the same way as in our previous study[7]. For the construction of our systems we started from the wurtzite structure of ZnO with experimental[20–23] lattice parameters $a = 3.2495$ Å, $b = 5.2069$ Å and $u = 0.3825$ Å. The ideal ZnO($000\overline{1}$) surface can be obtained by cutting this ideal bulk structure orthogonal to the c-axis. Due to the remaining dipole moment along the c-axis, this is a Tasker type 3 polar surface[24] and needs to be stabilized. In our model the stabilisation is done by a hydrogen coverage of 50% (1 H in a distance of 0.95 Å over each second oxygen atom), which should be the most stable configuration under catalytic conditions[25]. The same amount of counter ions is added to the Zn-terminated surface, i.e. one additional charge at a distance of 1.04 Å below each second Zn^{2+} ion. For these additional ions at the oxygen and zinc terminated surface we assumed charges of ± 0.9414 a.u.

Based on this structure, small hemispherical clusters (quantum clusters) were cut out of the ZnO($000\overline{1}$) surface. We used three clusters, which are shown in Fig. 1, as start structures. Cluster I is the same $Zn_{43}O_{44}H_{11}$ cluster which we used in Ref. 7, while cluster II consists of 43 zinc atoms, 44 oxygen atoms and 8 hydrogen atoms and is suitable to describe an oxygen vacancy between the OH rows at the surface, which differ in the surrounding hydrogen configuration. The large $Zn_{83}O_{83}H_{20}$ cluster (cluster III) is used for the investigation of double oxygen vacancies (V_{2H_2O}). From these start structures modified quantum clusters were generated by adding and/or removing atoms in order to obtain vacancy structures with (or without) adsorbates. These quantum clusters are embedded in a point charge field,

which consists of approximately 27000 individual point charges (the exact amount of point charges depends on the size of the quantum cluster and is 27470 for structures based on cluster I, 27473 for those based on cluster II and 27342 for all structures generated from cluster III).

In order to avoid an unphysical attraction of the electrons from the quantum cluster by the positive embedding point charges, we used a $28e^-$ effective core potential (ECP)[26] for the cations (Zn^{2+}) in the direct neighbourhood of the quantum cluster to model the repulsion caused by the missing core electrons.

All our calculations were done with the TURBOMOLE program package[27,28]. The atoms of the quantum cluster were described with all electron density functional theory. As exchange correlation functional the well known Perdew-Burke-Ernzerhof (PBE) functional[29] was chosen, which has been shown to give an accurate description of the ZnO structure[30]. First of all, we performed geometry optimizations[31] with a small split valence basis with a single set of polarization functions (SVP)[32], which consists of 3s2p1d contracted basis functions for O and C, 2s1p for H and 5s3p2d for Zn. Only the coordinates of atoms at the border were kept fixed (about half of the atoms in the quatum cluster). Afterwards we used the optimized structures to compute the hessian matrix and dipole gradients by numerical differentiation of the gradients and dipole moments with a step width of 0.02 a.u., to obtain normal modes and harmonic frequencies and IR intensities[33]. We also obtained the zero point vibrational energy E_{ZPVE} from the harmonic frequencies.

To compare the calculated frequencies with experimental measurements, one has to correct for errors due to the harmonic approximation and due to the chosen exchange correlation functional and basis set. This can be achieved by scaling the calculated wave numbers with predetermined empirical correction factors. Although there are scaling factors available in the literature (e.g. in Ref. 34), we decided to go another way, because such scaling factors depend on the kind of the normal mode, for example, CO stretch frequencies need a much lower value than those of deformation modes. Hence, we chose a set of 22 small (mainly organic) molecules (H_2O, CH_3OH, H_2CO, CH_4, acetone, ethane, ethene, CO, CO_2, HF, LiH, HCOOH, methyl formate, dimethyl ether, acetaldehyde, ethynol, 2-propenal, propan, methylacetate, ZnO_2, ZnH_2, HgH_2) with normal modes similar to those we want to investigate. We then calculated the harmonic vibrational frequencies of 108 normal modes of

the molecules in this set and scaling factors to match best experimental measurements[35–39]. In this way we obtained an average scaling factor of 1.004. We also determined individual scaling factors for the kinds of vibrational modes, which are most important for the present work, by averaging the correction factors only over the modes of the corresponding type. This gave us the following individual scaling factors: 0.988 for CH, 0.998 for CC, 0.979 for CO, and 0.994 for OH stretch modes and 1.027 for deformation modes of bonds between oxygen, hydrogen and carbon atoms. For all normal modes, which do not fit to one of these types, e.g. Zn-H or H-H stretching modes, we applied the above mentioned average scaling factor of 1.004.

While the small SVP basis set is sufficient for the calculation of vibrational frequencies, a larger basis set is needed to confirm the geometry and to calculate better converged bond lengths and energies of the systems. For this purpose we performed geometry optimizations using a triple zeta valence basis set with two sets of polarization functions (TZVPP)[40,41], which consists of 5s3p2d1f contracted basis functions for O and C and for H and Zn of, respectively, contracted 3s2p1d and 6s4p3d1f functions.

For all species discused in the current paper, the TZVPP optimized structure differs only slightly from the one obtained in the SVP basis. The maximum displacement of an atom in any of the structures is less then 0.2 Å.

From the electronic energies obtained with the TZVPP,E_{TZVPP}, basis and with the zero point vibrational energy E_{ZPVE} we calculated enthalpies H as:

$$H = E_{\mathrm{TZVPP}} + E_{\mathrm{ZPVE}} + E_{\mathrm{trans}} + E_{\mathrm{rot}} + p \cdot V$$

The translational (E_{trans}), rotational (E_{rot}), and $P{\cdot}V$ contributions have been evaluated for a temperature of 500 K, which is a typical temperature of the methanol synthesis[3,8,11,42]. This gives $E_{\mathrm{trans}}+E_{\mathrm{rot}}+pV = 14.55$ kJ mol^{-1} for linear and $E_{\mathrm{trans}}+E_{\mathrm{rot}}+pV = 16.63$ kJ mol^{-1} for non-linear molecules. Note that for bulk species the rotational and translational contributions vanish.

We also calculated entropies (S) for the same temperature and a pressure of $P = 4.1$ MPa, assuming a gas phase consisting of 73% H_2, 11% CO and 16% N_2, but also of CO_2, CH_2O and H_2O as side products in a concentration of 1 ppm. By doing so, we intended to model the

conditions of the catalytic methanol synthesis over ZnO. These are the same environmental conditions that were used in the experimental work for deriving the Bochum model[8]. In order to evaluate which species are energetically preferred under catalytic conditions, Gibb's enthalpies were calculated as $G = H - TS$ from the enthalpies and entropies.

III. RESULTS AND DISCUSSION

A. CO

The optimized geometries of the energetically most stable CO species found are shown in Fig. 2.In Tab. I we collected their vibrational frequencies and enthalpies of formation. In the same Table also the CO bond length of each species d(CO) and the CO adsorption enthalpy ΔH_{ads} are listed. The latter have been calculated as the difference of the formation enthalpies of the respective system with (ΔH_f(CO at cluster)) and without CO adsorbed(ΔH_f(cluster)).

$$\Delta H_{ads}(\text{CO at cluster}) = \Delta H_f(\text{CO at cluster}) - \Delta H_f(\text{cluster}) - \Delta H_f(\text{CO})$$

Above the defect free ZnO($000\overline{1}$) surface, only a physisorbed species (2.a) is stable. 2.b and 2.c are species resulting from the adsorption of CO at an F^{2+} vacancy. One can see that structure 2.b is a quite stable chemisorbed species. But the O-down variant (2.c) is a clearly only physisorbed. This supports the result of earlier calculations by Fink[43], which predicted the C-down structure to be slightly preferred at F^{2+} vacancies. One could assume, that the prediction of the C-down preference might be a result of the wrong description of the weak CO dipole moment by PBE. To check this, we also calculated for both species the second order Møller-Plesset perturbation theory (MP2) energies, within the SVP basis set, with the ricc2 module[44] of TURBOMOLE. The C-down species has a 34 kJ mol^{-1} lower MP2 energy than species 2.c, which confirms the PBE results.

Above an F vacancy we could only find one physisorbed species (Fig. 2.d) with a binding enthalpy of only -26 kJ mol^{-1}. Geometry optimizations from different start structures and structures with different locations of the hydrogen on the surrounding surface led to species,

which were similar to species 2.a, *i.e.* a CO physisorbed far offside the defect. No O-down species seems to be stable at an F vacancy, which was also found by Fink[43].

Another structure that might be of importance is formed by chemisorption of CO at a double oxygen vacancy (2.e and 2.f). Such a double oxygen vacancy (V_{2H_2O}) like species 3.h and 3.i can be interpreted as the result of the desorption of two water molecules which removes two neighbouring oxygen atoms from the defect free surface. The binding energy and stretch mode of this CO species are quite alike those of the species at a single F^{2+} vacancy. Similar to the single F^{2+} defect, also at such a double vacancy the C-down species (2.e) is energetically favored. The corresponding O-down species (2.f) is weakly physisorbed and shows a similar frequency for the CO stretch mode.

On ZnO powder samples CO is known[45,46] to absorb primarily at Zn^{2+} sites on the mixed terminated ZnO($10\overline{1}0$) surfaces where it exhibits a CO stretch frequency which is blueshifted relative to gas phase CO. A better reference for the present calculations for CO on the ZnO($000\overline{1}$) surface are experiments on single crystal surfaces where contamination with species on ZnO($000\overline{1}$) sites can be excluded. Recently H. Qiu and Y. Wang[47] performed HR-EELS and combined temperature desorption spectroscopy (TDS) and mass spectroscopy (MS) measurements at ZnO single crystals to obtain vibrational frequencies and adsorption enthalpies of CO adsorbed on ZnO($000\overline{1}$). The results are included in Tab. I. The measured CO stretch frequency is redshifted by 87 cm^{-1} compared to free CO. This is in good agreement with the calculated frequency of species 2.b (redshifted by 89 cm^{-1} with respect to free CO) and also the calculated adsorption enthalpy is in good accord with the experimental result. However, the vibrational frequencies and adsorption enthalpies of species 2.a – 2.f are too similar (comp. Tab. I), in particular 2.b and 2.d, to draw from this comparison a definite conclusion on the state of the surface. Further investigations are needed to confirm this assignment.

B. CO_2

On most metal oxide surfaces, CO_2 tends to form carbonate structures and preferably binds to oxygen vacancies[48]. Both is also found for the ZnO($000\overline{1}$) surface. In Fig. 3 the optimized structures are shown, while in Tab. II the corresponding vibrational frequencies and

enthalpies are listed.

At the defect free surface, carbon dioxide binds rather weakly to a surface oxygen and forms a monodentate carbonate structure (3.a). A similar monodentate structure can occur next to an F vacancy (3.d). In both cases the length of the bond to the surface oxygen is with about 1.5 Å slightly longer than the two other CO bonds, which are of quite equal length and in the range of typical carbonate CO bond lengths. The π_u mode of the free CO_2 has become a C-out-of-plane mode, which we will denote as $\pi(CO_3)$. Compared to free CO_2, the symmetric OCO stretch frequency is redshifted by only ≈ 100 cm^{-1}. The weakening of the CO double bonds upon chemisorption as carbonate is reflected in a redshift of the asymmetric stretch mode of more than 600 cm^{-1}. These monodentate structures are clearly favored over weakly adsorbed linear species.

Stable physisorbed CO_2 species were only found near oxygen vacancies at the ZnO$(000\overline{1})$ surface (3.c and 3.f). These species show CO bond length and vibrational frequencies very similar to those of free CO_2 — a fact that underlines the weak interaction of the adsorbate with the surface in this case. At F^{2+} vacancies one oxygen atom of carbon dioxide binds to the vacancy and is positioned near the center above the vacancy, with the bond axis of the linear CO_2 molecule forming an angle of about 53° with the surface (3.c). Such a weak coordination of linear CO_2 to the surface zinc atoms has already been suggested by Saussey[49]. Reduction of the defect to an F vacancy inhibits weak coordination of CO_2 due to the increased electron density. Therefore the CO_2 is in this case oriented parallel to the surface in greater distance to the vacancy (3.c). Alternatively the carbon atom can interact with a Zn atom of the F vacancy and form an energetically unfavorable Zn-CO_2 species (3.e) with a ZnC bond length of 2.0 Å. One oxygen atom of this species coordinates with the other two Zn atoms of the vacancy. The Mulliken charge[50] of the carbon atom of this species is +0.004 (the carbon atom of free CO_2 has a Mulliken charge of +0.329) and the whole CO_2 has a net charge of −0.687. This indicates that the carbon dioxide is reduced and therefore species 3.e is a carboxy species. This explains also why this species exhibits a characteristic carbonyl stretch mode at 1527 cm^{-1} instead of an asymmetric OCO stretch mode.

At F^{2+} vacancies also a bidentate carbonate species (3.b) can be formed, in which, similar to the Zn-CO_2 species, one oxygen is coordinated by two zinc atoms of the vacancy. Hence,

again a carbonyl stretch mode results. But in this case the C-O bond is much stronger and its wave number is with 1792 cm^{-1} clearly blueshifted.

Another polydentate carbonate structure which we investigated, is a tridentate carbonate with a planar structure (3.g) at a V_{2H_2O} vacancy (3.h). Such a double vacancy can formally be interpreted as the product of the desorption of two water molecules from the surface, which, due to the broken bonds, is a quite endothermic process. Nevertheless, CO_2 can adsorb at such a double vacancy with a large adsorption enthalpy, forming a tridentate carbonate species. In this variant both oxygen atoms of the adsorbate sit nearly at the positions of the missing surface oxygen atoms and the carbon atom binds to a surface oxygen atom. All three C-O bond lengths are nearly identical and the symmetric OCO stretch mode of the free molecule becomes a symmetric CO_3 stretch mode ($\nu(CO_3)$) with contributions from all three bonds. This mode has a wave number of 1034 cm^{-1} and a weaker IR intensity than the other stretch modes. Because bidentate carbonates exhibit a similar redshifted stretch frequency, this can be seen as a characteristic feature of polydentate carbonates. The asymmetric stretch frequency of the tridentate species is strongly redshifted and clearly dominated by the stretch of the two longer C-O bonds (1.31 Å and 1.32 Å), while the shortest bond is associated with a carbonyl-like CO stretch mode at 1539 cm^{-1}.

In summary, all three kinds of carbonates can be distinguished easily by their vibrational spectra, which can be seen in Fig. 4.

Qiu[51] confirmed the formation of polydentate carbonates at a single crystal ZnO($000\overline{1}$) surface after exposition to carbon dioxide in combined TDS and MS experiments. When he exposed the single crystal surface to $C^{18}O_2$ at low temperature, he observed $C^{16}O_2$ and $C^{18}O^{16}O$ aside $C^{18}O_2$ after thermal desorption. The oxygen exchange can only be understood if $C^{16}O_2$ is the desorption product of polydentate surface carbonates. Indeed there seems to be a weakly bound monodentate species (desorbing at lower temperature), which dominates at high coverages, and probably two polydentate species with larger binding energies. This is in accordance with our findings. Especially, when considering that such an exchange of adsorbate and surface oxygen atoms becomes the more likely, the more equivalent the three C-O bonds of the carbonate species are. Already a look at the C-O bond lengths shows that this similarity increases from monodentate to bidentate and tridentate carbonates.

Indeed, recent infrared studies at ZnO powders and high resolution low-energy electron loss spectroscopy measurements at single crystal surfaces by Noei *et al.*[52], suggest the formation of carbonates at ZnO(000$\overline{1}$) surfaces after CO_2 exposure. The authors observed a dominant carbonate species with bands at 1292 cm^{-1} and 1621 cm^{-1} (respectively 1293 cm^{-1} and 1615 cm^{-1} in the HR-EELS experiment) and a minority species with bands at 1313 cm^{-1} and 1543 cm^{-1}, which appears at higher temperature and seems to be stronger bound to the surface. The latter two frequencies fit quite well to a tridentate species (3.g), while the observed bands of the dominant species can be assigned to a monodentate species, although our DFT calculations seem to overestimate the ν_{asym}(OCO) wave number. Furthermore Noei *et al.* observed the characteristic $\pi(CO_3)$ mode at 850 cm^{-1} and a stretch mode at 1000 cm^{-1}, which we assign to polydentate carbonates like species 3.g or 3.b. This gives further proof of the formation of polydentate carbonates. Noei *et al.* also observed a physisorbed, linear CO_2 species with IR-bands at 2352 cm^{-1} and 638 cm^{-1} after exposition of ZnO powders to CO_2 at low temperature (below 180 K), in agreement with the present calculations (species 3.c and 3.f).

C. Formate, Formyl and Hydroxymethylene

We investigated formate, formyl and hydroxymethylene species at the ZnO(000$\overline{1}$) surface, which are possible intermediates or side products of the methanol synthesis. Calculated vibrational frequencies and formation enthalpies of formate, formyl and hydroxymethylene species are collected in Tab. III – V. Cutouts of the corresponding equilibrium structures are displayed in Fig. 5 – 7.

The carbonyl oxygen of the formate species (5.g) at the defect free ZnO(000$\overline{1}$) surface coordinates to a surface hydrogen, and forms a monodentate H-bonded structure. Also at F^{2+} centers, the carbonyl oxygen can coordinate to a hydrogen atom of a surface OH group (5.a). Compared to the species at the defect free surface, this monodentate species has a 65 cm^{-1} larger splitting between the CO stretch frequency ν(CO) and the OCO asymmetric stretch frequency ν_a(OCO). Beside this monodentate species, also a bidentate species (5.b) can occur at F^{2+} centers, if the carbonyl oxygen atom coordinates to a zinc atom at the vacancy. Such a bidentate species exhibits a symmetric OCO stretch mode ν_s(OCO) instead

of a CO stretch mode for the bond between the surface oxygen and the carbon atom. The splitting between this symmetric and the asymmetric stretch frequencies of such bidentate species is 418 cm^{-1} smaller than the splitting between ν(CO) and ν_a(OCO) of the monodentate species, which is a characteristic feature of these structures. According to the formation enthalpies, the bidentate species are energetically favored at F^{2+} centers. Reducing the vacancy by hydrogen adsorption, which increases the electron density at the vacancy, makes an attractive interaction with the carbonyl oxygen impossible, and therefore only monodentate formate species occur at F (5.c – 5.d) and at F^{2-} centers (5.e – 5.f). These species show spectra with frequencies quite close to those of the monodentate species at the defect free surface (5.g), a fact which makes it difficult to distinguish them by their vibrational spectra.

The comparison of these results with experimental results from the literature for formate species at ZnO($000\overline{1}$) single crystall surfaces[53] and at ZnO nanoparticles[18], which are included in Tab. III, suggests that both, monodentate and bidentate, formate species, have been observed.

For comparison, we also investigated possible adsorption sites for formic acid. We could find two chemisorbed species (5.h and 5.i), which have low formation enthalpies. In species 5.h the adsorbate's hydrogen binds to the F center, which leads to a strongly redshifted OH stretch mode at 2993 cm^{-1}. Furthermore an OH deformation band at 1203 cm^{-1} and an OCO scissoring frequency at 1336 cm^{-1} with weak IR intensities occur. A similar species can be formed on the defect free surface (5.i), when formic acid is deprotonated and coordinates to three neighbouring surface hydroxy groups. The transferred proton is still interacting with the adsorbate's oxygen (distance 1.3 Å) and is only weakly bound to the surface oxygen (distance 1.1 Å). This results in an extremely redshifted OH stretch frequency at 1719 cm^{-1}. The other two surface OH groups, which are interacting with the adsorbate by weak hydrogen bonds (distances 1.9 Å – 2.0 Å), exhibit stretch modes with 3257 cm^{-1} and 3304 cm^{-1}. The CO stretch frequency is slightly increased.

The most stable formyl species at F^{2+} centers are those (in Figs. 6.a – 6.c), where the carbon atom binds to two zinc atoms at the vacancy and the formyl oxygen atom binds to the third zinc atom at the vacancy. The frequencies are quite independent from the surrounding hydrogen configuration, except that species 6.b shows a slightly blueshifted CO stretch frequency due to interactions with the hydrogens of the nearby surface hydroxyl

groups.

At F centers formyl species occur (6.d – 6.f), which have quite different structures compared to the species at F^{2+}centers. Here the carbon atom exhibits only a bond to one zinc atom of the vacancy and the formyl oxygen atom forms hydrogen bonds with close-by surface OH groups. In this species the CH bond is weakened, so that a redshifted CH stretch band results. The CO stretch frequencies tend to be slightly redshifted, apart from species 6.c.

It has been suggested in Ref. 5 that in the methanol synthesis a subsequent intermediate of a formyl species, and a preliminary stage of a formaldehyde species, could be a hydroxymethylene species (7.a – 7.c). Species 7.a is quite similar to formyl species at F^{2+} centers, because the carbon atom is bound to two zinc atoms of the vacancy, while the (here protonated) oxygen atom coordinates with the third zinc atom at the vacancy. This weak polar interaction also weakens the strength of the formyl O-H bond, which leads to a slightly red-shifted OH stretch frequency. Species 7.b and 7.c differ from this variant, since here the carbon atom is bound to all three zinc atoms of the vacancy. The hydrogen atom of the OH group of these formyl species is oriented towards a nearby surface oxygen atom. Due to repulsion with surface hydroxyl groups, the CH and OH bending modes have frequencies which show a strong dependence on the surrounding hydrogen configuration of the surface. The strong coupling of the bending modes of species 7.c may be of interest, because here one observes symmetric and asymmetric coupled OH and CH bending modes instead of individual modes. All three species show CO stretch frequencies below 1000 cm^{-1}, typical for C-O single bonds. Species 7.b, which has the lowest CO stretch frequency, shows a strong interaction with a nearby surface hydroxyl group due to a hydrogen bond. This leads to a weakening of the OH bond of this group, which is reflected in the low stretch frequency of 3335 cm^{-1}.

D. Formaldehyde, Acetale and Hydroxymethyl

Physisorbed formaldehyde (8.a – 8.d) interacts via hydrogen bonds with surface hydroxyl groups. Alternatively, formaldehyde can abstract a hydrogen atom from a surface hydroxyl group and chemisorb as hydroxymethyl species (8.e – 8.h). At F^{2+} centers a physisorbed formaldehyde is attracted by the positively charged vacancy and reacts into an acetale

species (8.i – 8.k). Formaldehyde, hydroxymethyl and acetale species can be distinguished by their CH_2 deformation modes and their CO, respectively OCO, stretch modes. Because of the typically weak IR intensity of CH_2 deformation modes, rather the latter are applicable for assigning the experimental spectra. In Tab. VI formation enthalpies and vibrational frequencies of these species are listed. Cutouts of the equilibrium structures are shown in Fig. 8.

The formaldehyde species at the defect free surface (8.a) is no longer planar — as is free formaldehyde. Due to a weak bond between the carbon atom and a surface oxygen, which has a stretch frequency of 669 cm^{-1}, the OCO angle is 110° and the HCH angle is 109.6°. The distance between the carbon atom and the surface oxygen is with 1.55 Å a little bit longer than a typical C-O single bond. This deformation effects the vibrational modes as follows: it leads to a weakening of the carbonyl bond and redshifts the corresponding stretch frequency by 350 cm^{-1}. The CH_2 wagging mode has now a 338 cm^{-1} higher wave number. Furthermore, this species exhibits a new twisting mode ($\tau(CH_2)$) and has an unusually low splitting of the symmetric and asymmetric CH_2 stretch modes.

At F centers, physisorbed formaldehyde is stabilized by hydrogen bonds from the carbonyl oxygen to surface hydrogen atoms (8.b and 8.c). Since the carbon atom is no longer coordinated to a surface O atom as in 8.a, the structure of the formaldehyde molecule remains (almost) planar. Hence the IR spectrum of this species is very similar to that of free formaldehyde.

A very different situation is met at F^{2-} centers, where the vacancy is reduced enough to allow a weak binding interaction between a zinc atom of the vacancy and the carbon atom of adsorbed formaldehyde, so that in this case the adsorbate (8.d) is bent again. This leads again to a weakening of the carbonyl CO bond and the CO stretch mode is shifted to lower frequencies. Also the hydrogen bonds from the adsorbate's oxygen to the surface hydrogens are strengthened, which strongly redshifts the wave numbers of the OH stretch modes of the surface hydroxyl groups to 2408 cm^{-1} and 2976 cm^{-1}, and blueshifts the OH bending frequencies to 1287 cm^{-1}. This increase of the hydrogen bond strengths is also reflected by the short distance from the adsorbate's oxygen to the nearest surface hydrogen of 1.55 Å. Deformation and stretch modes of these OH groups couple with the CH_2 deformation and stretch modes, which underlines the increased OH binding interaction.

Hydroxymethyl species can be formed at F^{2+} (8.e and 8.f) and at F centers (8.g and 8.h). They are characterized by low CO stretch frequencies and larger wave numbers for the CH_2 wagging mode. At F^{2+} centers, the hydroxymethyl's carbon atom is bound to a zinc atom of the vacancy. Weak polar interactions of the adsorbate's hydroxyl group to a surface oxygen atom and a surface hydrogen (8.e) or from it's oxygen atom to a surface zinc atom (8.f) lead to a further stabilization. In the former case (8.e), the stretch frequency of the surface OH group is redshifted to 3138 cm^{-1}, while species 8.f shows a higher OH stretch frequency at 3542 cm^{-1}— probably because here the hydrogen atom is not coordinated to a surface oxygen and therefore the OH bond strength is not weakenend. This also explains why the OH bend mode of this species has a frequency in the region of free CH_2OH instead at $\approx$ 1508 cm^{-1}, which is the typical value for most other hydroxymethyl species.

At F centers, the bond of the adsorbate's carbon atom to the surface oxygen is nearly perpendicular to the surface, just like it is the case for species 8.a. Thereby a CH_2 twisting mode arises and the CH_2 wagging frequencies are blueshifted. While these species (8.f and 8.g) have higher CO stretch frequencies, their OH stretch mode is predicted at lower frequencies (2916 cm^{-1}, respectively even 2554 cm^{-1}). The bond to the surface oxygen is also no longer a weak bond, which leads to CO stretch frequencies at 902 cm^{-1} and 898 cm^{-1} respectively.

Acetale species (8.i – 8.k) can only occur at F^{2+} centers, because only in this case no repelling negative charge is located at the vacancy. These species exhibit symmetric and asymmetric OCO stretch modes with low wave numbers, while all other wave numbers are close to those of hydroxymethyl species at F centers, with the exception of the missing OH bend and stretch modes of the adsorbate. The formation enthalpies of the acetale species depend strongly on the surrounding hydrogen configuration due to the repulsion between the hydrogen atoms of the CH_2 group and surface hydroxyl groups. The less repelling hydrogen atoms are present in the local surrounding of an acetale, the lower is its formation energy.

E. Methoxy species

We investigated different physisorbed methanol and chemisorbed methoxy species at the ZnO($000\bar{1}$) surface (see Fig. 9 for cutouts of the optimized geometries and Tab. VII for their

vibrational frequencies and enthalpies of formation).

Physisorbed methanol species can be found above the defect free surface (9.a) and above F vacancies (9.b). They are stabilized by hydrogen bonds to surface oxygen atoms and to hydrogen atoms of surface hydroxyl groups. Thus, in both cases the O-H bond of the adsorbate's hydroxy group is weakened due to the interaction with a surface oxygen atom (the distance of the adsorbate hydrogen atom to the surface oxygen is 1.7 Å), which leads to an extremely redshifted OH stretch frequency of 2588 cm^{-1} for species 9.a and of 2447 cm^{-1} for species 9.b, compared to free methanol, for which the calculated (and scaled) wave number is 3694 cm^{-1}. Similar, the OH stretch frequencies of the interacting surface OH groups are shifted to lower frequencies (3332 cm^{-1} – 3460 cm^{-1}), compared to those of the adsorbate free surface (see Tab. VIII).

At F^{2+} centers methanol adsorbs dissociatively by transferring the proton of the alcohol group to a surface oxygen atom, leaving a methoxy species at the vacancy. Thereby the methoxy anion fills the oxygen vacancy of the defect (9.d – 9.e). Species 9.c is an intermediate on the reaction pathway from methanol to such a methoxy species. The adsorbed methanol coordinates to a Zn cation of the vacancy, and the adsorbate's proton – still bound to the adsorbate with a bond length of 1.01 Å – is already oriented towards the nearest surface oxygen and forms a hydrogen bond, which is 1.79 Å in length. Also in this case, the result of the interaction is a strongly redshifted OH stretch frequency of 2370 cm^{-1}.

Structures 9.d and 9.e are very stable and indeed methanol reacts at an F^{2+} vacancy without reaction barrier to these methoxy species[7]. This is totally different for methoxy species at F centers (9.f – 9.g), for which the desorption enthalpies are much smaller and which therefore react more easily to methanol. This means that the reaction of a methoxy species at an F^{2+} center into physisorbed methanol can only be achieved if the vacancy is first reduced by hydrogen, followed by the reaction of the resulting methoxy species at an F center into methanol.

Methoxy species at F^{2+} and F centers have similar frequencies with differences smaller than 30 cm^{-1} and also the surrounding hydrogen configuration has only a similar small influence on the vibrational frequencies, so that one can not easily distinguish between the individual adsorption in IR spectra. Nevertheless, we can clearly support the assignments for bands of

methoxy species at ZnO surfaces from IR measurements at ZnO nanoparticles in Ref. 18.

IV. SUMMARY AND CONCLUSION

We have calculated vibrational frequencies and formation enthalpies of possible educts, intermediates, spectator species and side products of the methanol synthesis at the ZnO$(000\overline{1})$ surface.

Carbon monoxide is on the defect free surface only weakly physisorbed, but chemisorbs at F^{2+} and F centers in a C-down geometry, which leads to a redshift by 62 cm^{-1} – 81 cm^{-1} compared to free CO. Carbon dioxide forms monodentate and bidentate carbonate species at oxygen vacancies, and even a tridentate species at a double oxygen vacancy might be possible. These species differ especially in the CO and OCO stretch frequencies, which is in agreement with experimental findings[51]. Furthermore, they can be clearly distinguished from physisorbed linear species, which can also occur as confirmed by recent IR measurements[52]. At F^{2+} centers bidentate formate species are energetically slightly favourable. They can be clearly distinguished from the monodentate variant by the redshifted symmetric OCO stretch frequency and the symmetric OCO stretch mode at 1295 cm^{-1}, which only bidentate species exhibit in contrast to typical CO stretch frequencies between 1072 cm^{-1} and 1119 cm^{-1} of monodentate variants. At reduced oxygen vacancies and at the defect free surface, only monodentate species are formed. Formyl species were mainly formed at F centers and show redshifted CH stretch bands below 2800 cm^{-1} and CO stretch frequencies of 1424 cm^{-1} – 1478 cm^{-1}. Hydroxymethylene species, which are possible intermediates between formyl and formaldehyde species, show spectra which are sensitive to their environment. Formaldehyde can bind weakly in a planar geometry at F centers or in a slightly bent geometry at the defect free surface or at F^{2-} centers. The bended structures seem to result from a transfer of electron density from the surface to the adsorbate's carbon atom, leading to a carbanion like species with redshifted CO and CH_2 stretch frequencies and differences in the CH_2 deformation bands. At F^{2+} centers, formaldehyde reacts into an acetale with characteristic low symmetric and asymmetric OCO stretch modes below 1021 cm^{-1}. Hydroxymethyl species have slightly higher formation enthalpies than formaldehyde species, but differ in their spectrum not only due to OH stretch and deformation modes, but also

by redshifted CO stretch frequencies of 984 cm^{-1} – 1126 cm^{-1}. The calculated frequencies of methoxy species at oxygen vacancies, obtained in this work, are in good agreement with experimental findings, but due to their rather weak dependence on the surrounding hydrogen configuration and the oxidation state of the vacancy, one can not clearly distinguish between the species at F^{2+} and F centers and assign their experimental spectra.

Some of the species for which we have computed and discussed above the vibrational spectra have already been observed in experimental studies. In most cases the agreement between the experimental spectra and the results of the DFT calculations is very good. For other species we predicted in this theoretical study for the first time IR spectra which might be helpful for their experimental identification and the assignment of their spectra.

ACKNOWLEDGMENTS

The present work was supported by the Deutsche Forschungsgemeinschaft (DFG) within the framework of the Collaborative Research Center 558 "Metal–Substrate Interactions in Heterogeneous Catalysis" (SFB 558) and by the Fonds der Chemischen Industrie. We acknowledge the fruitful cooperation with Yuemin Wang, Hengshan Qiu and Heschmat Noei.

SUPPLEMENTAL MATERIAL

The formation enthalpies, unscaled vibrational frequencies, IR intensities, and the cartesian coordinates of the equilibrium structures are available as supplemental material[54].

REFERENCES

[1]D. Cornthwaite, *UK Patent* **1966**, 1296212 (to ICI).

[2]J. Hansen, *Handbook of Heterogenous Catalysis*, vol. 4 (Wiley-VCH, Weinheim, 1997).

[3]H. Wilmer, M. Kurtz, K. Klementiev, O. Tkachenko, W. Grünert, O. Hinrichsen, A. Birkner, S. Rabe, K. Merz, M. Driess, et al., Phys. Chem. Chem. Phys. **5**, 4736 (2003).

[4]H. Kung, Catal. Rev. Sci. Eng. **22**, 235 (1980).

[5] J. Kiss, J. Frenzel, N. N. Nair, B. Meyer, and D. Marx, J. Chem. Phys. **134**, 064710 (2011).

[6] J. Kiss, A. Witt, B. Meyer, and D. Marx, J. Chem. Phys. **130**, 184706 (2009).

[7] G. Roßmüller, V. Kleinschmidt, J. Koßmann, and C. Hättig, J. Phys. Chem. C **113**, 1418 (2009).

[8] M. Kurtz, J. Strunk, O. Hinrichsen, M. Muhler, K.Fink, B. Meyer, and C. Wöll, Angew. Chem. Int. Ed. **44**, 2790 (2005).

[9] S. French, A. Sokol, S. Bromley, C. Catlow, S. Rogers, F. King, and P. Sherwood, Angew. Chem. Int. Ed. **40**, 4437 (2001).

[10] X. Yin and D. Leung, Energy & Fuels **19**, 305 (2005).

[11] J. Hansen, *Handbook of Heterogenous Catalysis* (Wiley-VCH, Weinheim, 1997), vol. 4, chap. Methanol Synthesis, pp. 2920–2949.

[12] T. Askgaard, J. Nørskov, C. Ovesen, and P. Stoltze, J. Catal. **156**, 229 (1995).

[13] L. Grabow and M. Mavrikakis, ACS Catal. **1**, 365 (2011).

[14] S. A. French, A. A. Sokol, S. T. Bromley, C. R. A. Catlow, and P. Sherwood, Topics in Catalysis **24**, 161 (2003).

[15] L. Berezina, V. Matyshak, V. Korchak, T. Burdeinaya, V. Tret'yakof, G. Lin, and A. Rozovskii, Kinetics and Catalysis **50**, 775 (2009).

[16] J. Vohs and M. Barteau, Surf. Sci. **176**, 91 (1986).

[17] D. Schadwick and K. Zheng, Catal. Lett. **20**, 231 (1993).

[18] K. Kähler, M. Holz, M. Rohe, J. Strunk, and M. Muhler, Chem. Phys. Chem. **11**, 2521 (2010).

[19] C. Au, W. Hirsch, and W. Hirschwald, Surf. Sci. **221**, 113 (1989).

[20] R. Wyckoff, *Crystal Structures*, vol. I (Interscience Publisher, New York, 1965).

[21] *Landolt-Börnstein, New Series III* (Springer-Verlag, Berlin, 1982).

[22] S. Abrahams and J. Bernstein, Acta Crytallogr. **B25**, 1233 (1969).

[23] T. Sabine and S. Hogg, Acta Crystallogr. **B25**, 2254 (1969).

[24] P. Tasker, J.Phys.C.: Solid State Phys. **12**, 4977 (1979).

[25] B. Meyer, Phys. Rev. B **69**, 045416 (2004).

[26] F. Schautz, H.-J. Flad, and M. Dolg, Theor. Chem. Acc. **99**, 231 (1998), without g-projectors, avialable via www.turbomole.com.

[27] R. Ahlrichs, M. Bär, M. Häser, H. Horn, and C. Kölmel, Chem. Phys. Lett. **162**, 165 (1989).

[28] *TURBOMOLE V6.2 2010, a development of University of Karlsruhe and Forschungszentrum Karlsruhe GmbH, 1989-2007, TURBOMOLE GmbH, since 2007; available from* `http://www.turbomole.com`.

[29] J. Perdew, K. Burke, and M. Ernzerhof, Phys. Rev. Lett. **77**, 3865 (1996).

[30] B. Meyer and D. Marx, Phys. Rev. B **67**, 035403 (2003).

[31] M. v. Arnim and R. Ahlrichs, J. Chem. Phys. **111**, 9183 (1999).

[32] A. Schäfer, H. Horn, and R. Ahlrichs, J. Chem. Phys. **97**, 2571 (1992).

[33] J. Neugebauer, M. Reiher, C. Kind, and B. Hess, J. Comp. Chem. **23**, 895 (2002).

[34] J. Merrick, D. Moran, and L. Radom, J. Phys. Chem. **111**, 11683 (2007).

[35] T. Shimanouchi, *Tables of Molecular Vibrational Frequencies Consolidated Volume I* (National Bureau of Standards, 1972).

[36] K. Huber and G. Herzberg, *Molecular Spectra and Molecular Structure IV. Constants of Diatomic Molecules* (Van Nostrand Reinhold Co., 1979).

[37] W. Person, *Vibrational Intensities in Infrared and Raman Spectroscopy* (Elsevier, Amsterdam, 1982).

[38] R. Hochstrasser and J. Wirz, Angew. Chem. **101**, 183 (1989).

[39] M. Jacox, J. Phys. Chem. Ref. Data **27**, 115 (1998).

[40] A. Schäfer, C. Huber, and R. Ahlrichs, J. Chem. Phys. **100**, 5829 (1994).

[41] F. Weigend, M.Häser, H. Patzelt, and R. Ahlrichs, Chem. Phys. Lett. **294**, 143 (1998).

[42] K. Kochloefl, *Handbook of Heterogenous Catalysis* (Wiley-VCH, Weinheim, 1997), vol. 4, chap. Methanol Synthesis, p. 183.

[43] K. Fink, Phys. Chem. Chem, Phys **8**, 1482 (2006).

[44] C. Hättig, A. Hellweg, and A. Köhn, Phys. Chem. Chem. Phys. **8**, 1159 (2006).

[45] H. Noei, C. Wöll, M. Muhler, and Y. Wang, Appl. Catal. A **391**, 31 (2011).

[46] D. Scarano, S. Bertarione, G. Spoto, A. Zecchina, and C. Areán, Thin Solid Films **400**, 50 (2001).

[47] Y. Wang, H. Qiu, and J. Koßmann, in preparation.

[48] U. Burghaus, Catal. Today **148**, 212 (2009).

[49] J. Saussey, J.-C. Lavalley, and C. Bovet, J. Chem. Soc., Faraday Trans. 1 **78**, 1457 (1982).

[50] R. Mulliken, J. Chem. Phys. **23**, 1833 (1955).

[51] H. Qiu, Ph.D. thesis, Ruhr-Universität Bochum, Bochum, Germany (2009), URL `http://www-brs.ub.ruhr-uni-bochum.de/netahtml/HSS/Diss/QiuHengshan/diss.pdf`.

[52]H. Noei, C. Wöll, M. Muhler, and Y. Wang, J. Phys. Chem. C **115**, 908 (2011).

[53]S. Crook, H. Dhariwal, and G. Thornton, Surf. Sci. **382**, 19 (1997).

[54]See Supplementary Material Document No. for formation enthalpies, unscaled vibrational frequencies, IR intensities, and the cartesian coordinates of the equilibrium structures. For information on Supplementary Material, see `http://www.aip.org/pubservs/epaps.html`.

[55]O. Gilliam, C. M. Johnson, and W. Gordy, Phys. Rev. **78**, 140–144 (1950).

[56]K. Huber and G. Herzberg, *Molecular Spectra and Molecular Structure IV. Constants of Diatomic Molecules* (Van Nostrand Reinhold Co., 1979).

[57]W. Person and G. Zerbi, *Vibrational Intensities in Infrared and Raman Spectroscopy* (Elsevier Scientific Pub. Co, Amsterdam, 1982).

[58]T. Nakanaga, S. Kondo, and S. Saeki, J. Chem. Phys **76**, 3860 (1982).

Table I. CO species at defects on the ZnO($000\overline{1}$) surfaces. Enthalpies of formation (ΔH_f) and adsorption (ΔH_{ads}) are given in kJ mol^{-1}, CO stretch frequencies (ν (CO)) in cm^{-1} and CO bond lengths (d(CO)) in Å. The second column specifies the defect which is either a single oxygen vacancy (F^{2+}, F, F^{2-}) or a V_{2H_2O} defect (like species 3.h and 3.i).

	defect	ΔH_f	ΔH_{ads}	ν (CO)	d(CO)
free CO, calc.	–	0	–	2115	1.14
free CO, exp.[36,55]	–	0	–	2143	1.13
2.a	none	−34	−34	2053	1.14
2.b	F^{2+}	220	−54	2026	1.14
2.c	F^{2+}	261	−10	2049	1.14
2.d	F	95	−26	2034	1.14
2.e	V_{2H_2O}	510	−54	2066	1.14
2.f	V_{2H_2O}	539	−25	2061	1.15
exp. CO at ZnO($000\overline{1}$)[47]	–	–	−53	2056	–

Table II. CO_2 species at defects on the ZnO($000\overline{1}$) surface. Enthalpies of formation (ΔH_f) and adsorption (ΔH_{ads}) are given in kJ mol^{-1}, vibrational frequencies in cm^{-1} and bond length (d(CO)) in Å. The second column specifies defect (comp. Tab. I).

	defect	ΔH_f	ΔH_{ads}	π	$\nu_{sym}(CO_2)$ / $\nu(CO_3)$	$\nu_{asym}(CO_2)$	ν (C=O)	d(CO)
free CO_2, calc.	–	0	0	642	1312	2370	–	1.17/1.17
free CO_2, exp.[35,56,57]	–	–	–	667	1333	2349	–	1.16/1.16
3.a (monodentate)	none	−39	−39	804	1231	1768	–	1.23/1.25/1.53
3.b (bidentate)	F^{2+}	236	−53	796	1011	–	1792	1.20/1.36/1.41
3.c (linear)	F^{2+}	239	−50	609	1288	2348	–	1.16/1.18
3.d (monodentate)	F	43	−34	800	1229	1750	–	1.23/1.25/1.52
3.e (Zn-CO_2)	F	166	38	781	1229	–	1527	1.25/1.31
3.f (linear)	F	91	−32	608	1296	2341	–	1.17/1.17
3.g (tridentate)	V_{2H_2O}	424	−139	803	1034	1332	1537	1.26/1.31/1.32

Table III. Vibrational frequencies of formate species at ZnO($000\overline{1}$)in cm^{-1} and the corresponding enthalpies of formation (ΔH_f) and Gibb's enthalpies (ΔG_f) in kJ mol^{-1}.

	defect	ν_s(OCO)	ν(CO)	δ(CH)	ν_{as}(OCO)	ν(CH)	ΔH_f	ΔG_f
free HCOOH	–	–	1081	1397	1777	3030	17	27
5.a	F^{2+}	–	1072	1368	1709	2933	244	188
5.b	F^{2+}	1295	–	1321	1505	2999	213	161
5.c	F	–	1145	1363	1681	2875	1	−8
5.d	F	–	1125	1371	1704	2899	4	−5
5.e	F^{2-}	–	1136	1359	1667	2875	98	115
5.f	F^{2-}	–	1136	1348	1669	2921	105	125
5.g	none	–	1119	1361	1691	2907	−39	36
5.h	F	–	1146	1414	1699	2928	−66	−82
5.i	none	–	1213	1379	1719	2843	−101	44
Exp., at ZnO[18]	–	1367	–	1380	1585	2962	–	–
Exp., at ZnO($000\overline{1}$)[53]	–	–	1080	1371	1605	2928	–	–

Table IV. Vibrational frequencies of formyl species at ZnO($000\overline{1}$)in cm^{-1} and the corresponding enthalpies of formation (ΔH_f) and Gibb's enthalpies (ΔG_f) in kJ mol^{-1}.

	defect	ν(CO)	δ(CH)	ν(CH)	ΔH_f	ΔG_f
6.a	F^{2+}	1521	1365	2733	130	128
6.b	F^{2+}	1478	1361	2757	145	145
6.c	F^{2+}	1532	1329	2768	134	132
6.d	F	1528	1307	2502	90	118
6.e	F	1424	1303	2420	112	142
6.f	F	1442	1319	2609	91	124

Table V. Vibrational frequencies of hydroxymethylene species at F centers on ZnO($000\overline{1}$) in cm^{-1} and formation enthalpies (ΔH_f and ΔG_f) in kJ mol^{-1}. The OH ($\delta(OH)_{bend}$) and CH ($\delta(CH)_{bend}$) bending normal modes of species 7.c are combined to one symmetric (δ_{sym}) and one asymmetric (δ_{asym}) deformation mode.

structure	ν(CO)	$\delta(OH)_{bend}$	$\delta(CH)_{bend}$	ν(CH)	ν(OH)	ΔH_f	ΔG_f
7.a	931	1208	1264	2872	3566	110	152
7.b	898	1345	1210	2829	3405	125	166
7.c	962	$\delta_{sym} = 1264$, $\delta_{asym} = 1489$		2899	3171	99	139

Table VI. Gibb's enthalpies of formation (ΔG_f) in kJ mol^{-1} and vibrational frequencies (in cm^{-1}) of formaldehyde (8.a – 8.d), hydroxymethyl (8.e – 8.h), and acetale species (8.i – 8.k) at ZnO$(000\overline{1})$. Frequencies listed: CO stretch (ν(CO)), CH_2 rocking ($\rho(CH_2)$), CH_2 scissoring ($\delta_{\mathrm{sciss}}(CH_2)$), wagging ($\omega(CH_2)$), symmetric ($\nu_{\mathrm{s}}(CH_2)$) and asymmetric ($\nu_{\mathrm{a}}(CH_2)$) CH stretch, and OH bend (δ(OH)).

	defect	$\omega(CH_2)$	$\rho(CH_2)$	$\tau(CH_2)$	$\delta_{\mathrm{s}}(CH_2)$	δ(OH)	ν(CO)	$\nu_{\mathrm{s}}(CH_2)$	$\nu_{\mathrm{a}}(CH_2)$	ΔG_f
free CH_2O, calc.	–	1027	1240	–	1474	–	1583	2839	2932	−46
CH_2O, exp.[58]	–	1167	1249	–	1500	–	1746	2782	2843	–
free CH_2OH	–	595	1048	–	1469	1352	1187	3004	3128	52
8.a	none	1365	1243	1118	1498	–	1233	2775	2812	30
8.b	F	1018	1247	–	1486	–	1612	2811	2893	-112
8.c	F	1021, 1044	1241	–	1477	–	1587	2824	2922	−73
8.d	F^{2-}	1025, 1067	1199	–	1418	–	1255	2753	2822	161
8.e	F^{2+}	1239	1103, 1169	–	1443	1508	984	2875	2962	103
8.f	F^{2+}	1242	1095	–	1452	1281	952	2880	2941	120
8.g	F	1394	1087, 1126	1249	1492	1508	1096	2860	2918,	27
8.h	F	1398	1087, 1129	1250	1495	1504	1126	2744	2909	32
8.i	F^{2+}	1380	1101	1243	1406	–	945[b], 776[a]	2924	3006	160
8.j	F^{2+}	1386	1130	1250	1472	–	1021[b], 904[a]	2875	2947	116
8.k	F^{2+}	1370	1111	1233	1446	–	940[b], 763[a]	2933	3014	92

[a] asymmetric OCO stretch frequency

[b] symmetric OCO stretch frequency

Table VII. Vibrational frequencies and formation enthalpies (ΔH_f and ΔG_f in kJ mol^{-1}) of methanol and methoxy species in comparison with available experimental results. All wave numbers are given in cm^{-1}. The following frequencies are listed: Bending ($\delta_{\mathrm{bend}}(CH_3)$), scissoring ($\delta_{\mathrm{sciss}}(CH_3)$), wagging ($\omega(CH_2)$) and twisting ($\tau(CH_2)$) modes of the methyl group as well as symmetric ($\nu_s(CH_3)$) and asymmetric ($\nu_a(CH_3)$) CH_3 stretch frequencies and the CO stretch frequency (ν(CO)).

	defect	ν(CO)	$\delta_{\mathrm{bend}}(CH_3)$	$\omega(CH_2)$	$\tau(CH_2)$	$\delta_{\mathrm{sciss}}(CH_3)$	$\nu_s(CH_3)$	$\nu_a(CH_3)$	ΔH_f	ΔG_f
9.a	none	1068	1450	1158	1175	1456, 1465	2876	2935, 2998	−222	−189
9.b	F	1057	1450	1161	1170	1458, 1466	2889	2956, 3012	−148	−196
9.c	F^{2+}	977	1446	1156	1170	1463, 1473	2924	3028, 3040	32	64
9.d	F^{2+}	988	1386	1178	1167	1457, 1468	2898	2989,3010	−107	−63
9.e	F^{2+}	1003	1425	1163	1175	1445, 1474	2892	2982	−81	−39
9.f	F	976	1412	1147	1158	1441, 1468	2887	2984, 3007	−77	−9
9.g	F	977	1405	1146	1152	1448, 1461	2879	2959, 2991	−76	−8
free CH_3OH, calc.	–	1067	1465	1070	1161	1454, 1465	2859	2896, 3008	−134	−101
free CH_3OH, exp.[35]	–	1033	1455	1060	1165	1477	2844	2960, 3000	–	–
at ZnO, exp[18]	–	1067	1468	–	–	–	2817	2932	–	–

Table VIII. The range of formation enthalpies (ΔH_f and ΔG_f) of the defect free ideal surface, of single oxygen vacancies (F^{2+} , F vacancies and F^{2-} vacancies) and of species 3.h and 3.i in kJ mol^{-1} and the range of OH stretch frequencies of nearby surface hydroxy groups in cm^{-1}.

	ΔH_f	ΔG_f	ν(OH)
ideal surface (no defect)	0	0	3673 – 3678
F^{2+} vacancy	270 – 353	150 – 227	3658 – 3679
F vacancy	64 – 144	−13 – 59	3660 – 3679
F^{2-} vacancy	142 – 189	98 – 132	3406 – 3678
V_{2H_2O} (species 3.h and 3.i)	563 – 565	299 – 303	3654 – 3661

Fig. 1: Visualization of the three quantum clusters (I, II, and III) used as start structures. Oxygen atoms are red, zinc atoms dark blue, carbon atoms grey and hydrogen atoms white colored. All clusters are shown in a top view (ZnO(000$\overline{1}$) surface) and a side view (looking at the (1000) plane). Additionally central cutouts for each of these clusters are shown which were used in the following figures to visualize the different adsorbate structures.

Fig. 2: Cutouts of equilibrium structures of CO species at the ZnO(000$\overline{1}$)-surface. Species (2.a) is a physisorbed CO molecule above the vacancy free ideal surface. (2.b) and (2.c) are adsorbed species at a F^{2+} vacancy, while (2.e) and (2.f) are species located at a double V_{2H_2O} vacancy (species 3.i). (For the color code see Fig. 1)

Fig. 3: Cutouts of equilibrium structures of CO_2 species and V_{2H_2O} vacancies at the ZnO(000$\overline{1}$)surface (For color code see Fig. 2). 3.a is a monodentate carbonate at the defect free surface, 3.b and 3.c are species at a F^{2+} vacancy, 3.d – 3.f are species at F centers and 3.g is a tridentate carbonate species at V_{2H_2O} vacancy (3.h). 3.h and 3.i are two examples for such a V_{2H_2O} defect. (For the color code see Fig. 1)

Fig. 4: Vibrational spectra of monodentate (species 3.a, red), bidentate (species 3.b, green), and tridentate (species 3.g, blue) carbonate species and schematic visualizations of the corresponding normal modes.

Fig. 5: Cutouts of equilibrium structures of formate species at F^{2+} (Fig. 5.a and Fig. 5.a), F (Fig. 5.c, Fig. 5.d and Fig. 5.h), and F^{2-} centers (Fig. 5.e and Fig. 5.f) and at the defect free ZnO(000$\overline{1}$) surface (Fig. 5.g and Fig. 5.i). (For the color code see Fig. 1)

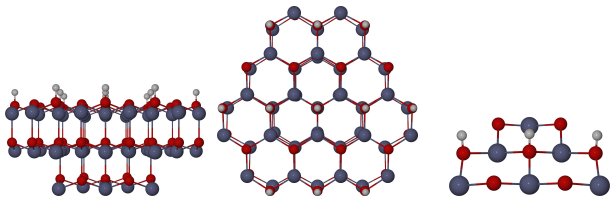
Fig. 6: Cutouts of equilibrium structures of formyl species at F^{2+} (Fig. 6.a – Fig. 6.c) and F (Fig. 6.d – Fig. 6.f) centers on ZnO(000$\overline{1}$). (For the color code see Fig. 1)

Fig. 7: Cutouts of equilibrium structures of hydroxymethylene species at F centers on ZnO(000$\overline{1}$). (For the color code see Fig. 1)

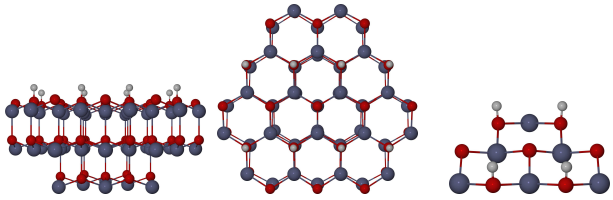
Fig. 8: Cutouts of equilibrium structures of formaldehyde (8.a – 8.d), hydroxymethyl (8.e – 8.h), and acetale species (8.i – 8.k) at ZnO(000$\overline{1}$). Acetale species only occur at F^{2+} centers,

formaldehyde species at the defect free surface (8.a), F (8.b and 8.c) and F^{2-} centers (8.d), and hydroxymethyl species at F^{2+} (8.e and 8.f) and F centers(8.g and 8.h). (For the color code see Fig. 1)

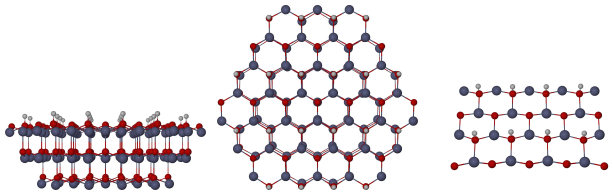
Fig. 9: Cutouts of equilibrium structures of physisorbed methanol and methoxy species. Fig. 7.a: methanol physisorbed at the defect free surface. Fig. 7.b: methanol physisorbed at F center. Fig. 7.c: methanol at F^{2+}center. Fig. 7.d, Fig. 7.e: methoxy at F^{2+} center. Fig. 7.f, Fig. 7.g: methoxy at F center. (For the color code see Fig. 1)



I (side view) I (top view) I (cutout)

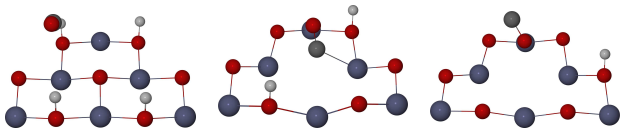


II (side view) II (top view) II (cutout)

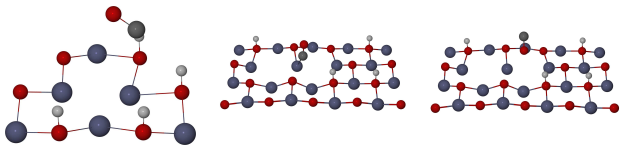


III (side view) III (top view) III (cutout)

Figure 1.

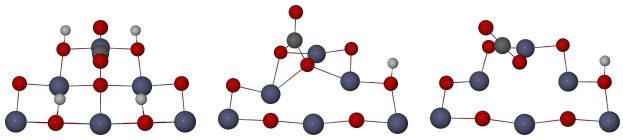


(2.a) (2.b) (2.c)

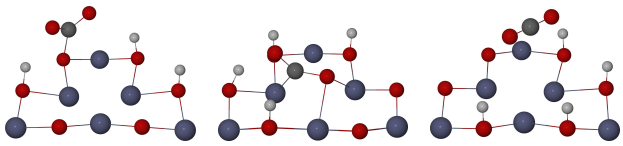


(2.d) (2.e) (2.f)

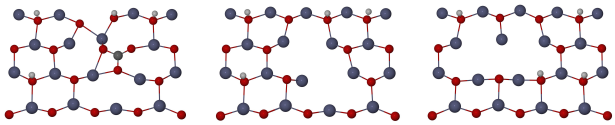
Figure 2.



(3.a) (3.b) (3.c)



(3.d) (3.e) (3.f)



(3.g) (3.h) (3.i)

Figure 3.

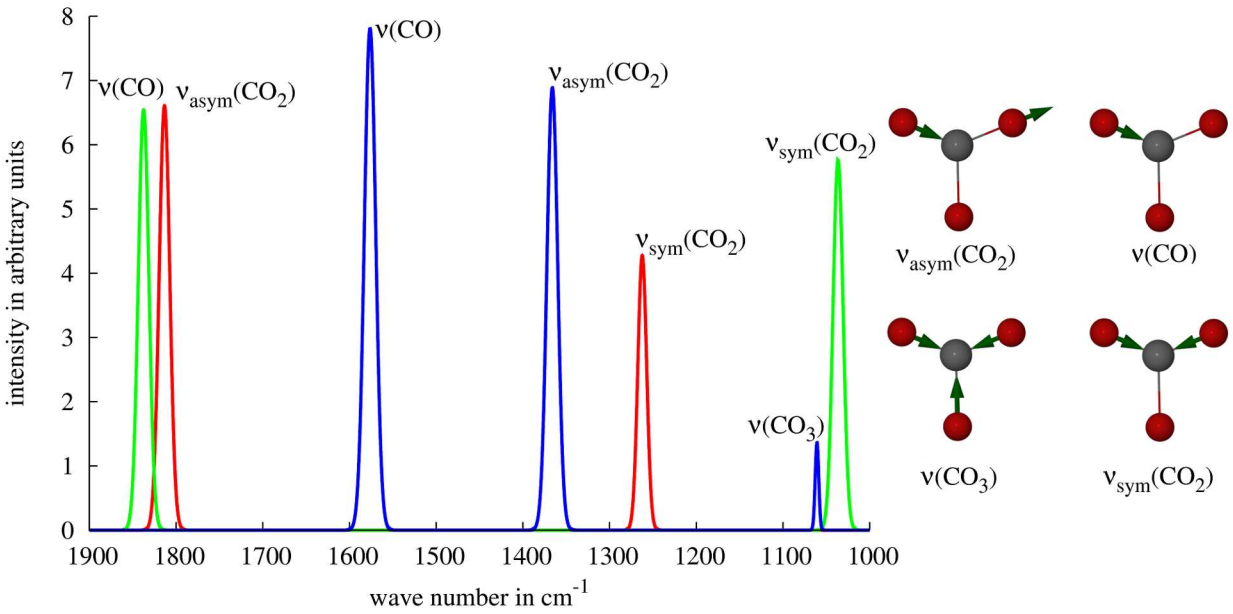


Figure 4.

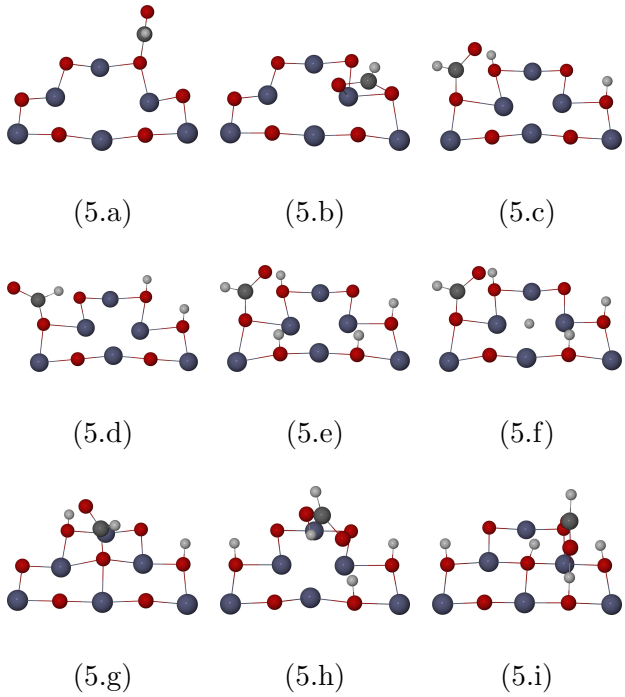
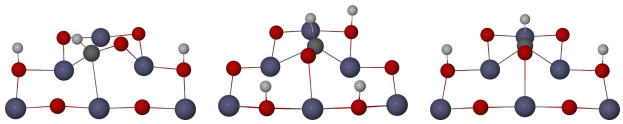
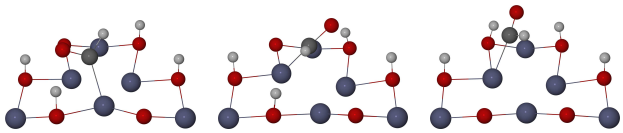


Figure 5.

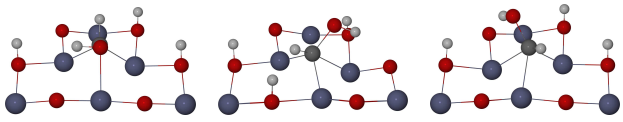


(6.a) (6.b) (6.c)



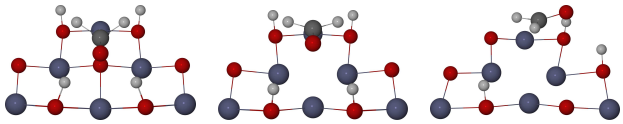
(6.d) (6.e) (6.f)

Figure 6.

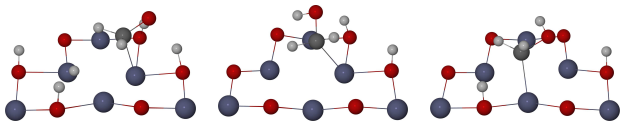


(7.a) (7.b) (7.c)

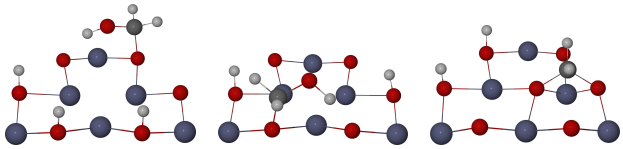
Figure 7.



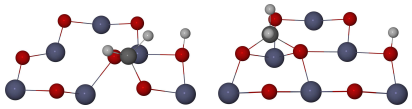
(8.a) (8.b) (8.c)



(8.d) (8.e) (8.f)

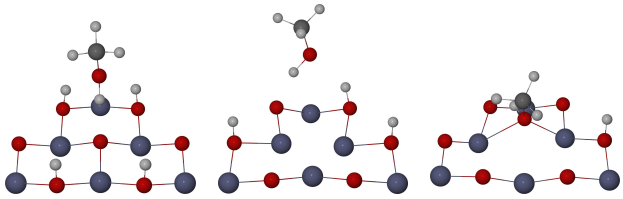


(8.g) (8.h) (8.i)

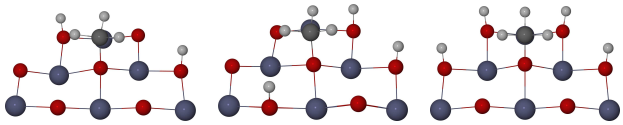


(8.j) (8.k)

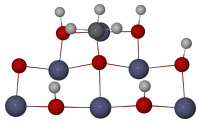
Figure 8.



(9.a) (9.b) (9.c)



(9.d) (9.e) (9.f)



(9.g)

Figure 9.